Tutor

Dr. Francesc Viñes Solana
Departament de Ciència de Materials i Química Física

Grau de Química

Treball Final de Grau

DFT Accuracy on Bulk Transition Metals Properties

Exactitud del DFT en la Descripció de Propietats de *Bulk* de Metalls de Transició

Andrea Fernández Martínez

January 2021

Universitat de Barcelona

B:KC Barcelona Knowledge Campus
Campus d'Excel·lència Internacional

El conocimiento descansa no solo sobre la verdad sino también sobre el error.

C. G. Jung

Doy las gracias de corazón a Judit, David, Martí, Mike y Andrea por haberme hecho esta etapa del camino más fácil. Sin vosotros mi vida en la universidad no hubiera tenido momentos tan felices. También doy las gracias a mis padres y mis hermanos por no haberme dejado abandonar el grado, sin vosotros no habría llegado hasta aquí. Gracias Jordi, por acompañarme en los momentos felices y sobre todo en los momentos difíciles que la vida nos ha dado. Por último, doy las gracias a Francesc Viñes por guiarme con paciencia y alegría en este Trabajo que pone fin al grado de Química.

REPORT

CONTENTS

1. SUMMARY

Density Functional Theory would be exact in estimating a polyelectronic chemical system energy, when the exchange-correlation (*xc*) functional would be known. Unfortunately, it is not, and has to be approximated, with dozens of *xc* functionals developed in the last decades, belonging to different rungs of Jacob's ladder of *xc* improvement. In the case of Transition Metals (*TMs*), mostly describing few late TMs and their structural properties. Recent studies expanded the analysis covering different bulk properties —the shortest interatomic bond distance, δ, the cohesive energy, E_{coh}, and the bulk modulus, B_0— and surface features —the surface energy, γ, the work function, ϕ, and the interlayer distances, Δ_{ij}—.

Here we carry out such performance evaluation on so far ignored *xc* functionals, either within the most basic local density approximations, including the, Hendin-Lundqvist (*HL*) and Perdew-Zunger (*PZ*) *xc* functionals, or within the Generalized Gradient Approximation (GGA), exploring the revised Perdew-Burke-Ernzerhof (r*evPBE*) and the Armiento-Mattson (*AM05*) *xc* functionals. Aside from these, the recent meta-GGA Strongly Constrained Appropriately Normed (*SCAN*) functional is analysed, characterized by fulfilling all 17 mathematical conditions an *xc* must comply, plus the Bayesian Error Estimation Functional (*BEEF*) is explored, a functional where artificial intelligence, in the form of a machine learning algorithm, was used to adjust the mathematical expression to a large and diverse set of experimental results.

The present results, acquired for 27 TM bulks in their crystallographic structures —body-centred cubic, face-centred cubic, and hexagonal close-packed—, reveal that none of the explored functionals is best in describing TM bulks, were Viñes-Vega (*VV*) excels, and highlighting that, while SCAN performance is acceptable, BEEF is not. When accounting for TM surface properties, acquired on 81 low-index Miller surfaces, the same situation applies, not improving the VV *xc* adapted for solids (*VVsol*).

Keywords: Density functional theory, Exchange-correlation functionals, Transition metals, Bulk properties, Surface properties, Accuracy.

2. RESUM

Si es coneixes el funcional de bescanvi i correlació (*exchange-correlation – xc*), la teoria del funcional de la densitat seria exacta per obtenir l'energia d'un sistema químic polielectrònic. Malauradament, no és així, i s'han generat dotzenes de funcionals aproximats a tal efecte. Aquests funcionals de bescanvi i correlació es classifiquen en diferents esglaons segons l'escala de Jacob; de manera que en pujar esglaons millora el funcional *xc*. En quant als estudis dels metalls de transició, s'han focalitzat en les propietats estructurals dels metalls tardans. Estudis recents han ampliat l'anàlisi a propietats del interior del material o *bulk* —la mínima distància d'enllaç, δ, l'energia cohesiva, E_{coh}, i el mòdul de bulk, B_0— així com característiques superficials —la tensió superficial, γ, la funció treball, ϕ, i les distàncies entre capes, Δ_{ij}—.

En aquest treball s'ha avaluat alguns funcionals *xc* menyspreats a la literatura, siguí dins de l'aproximació local de densitat, com el Hendin-Lundqvist (*HL*) i Perdew-Zunger (*PZ*), o dins de l'aproximació local de gradient generalitzat (*Generalized Gradient Approximation – GGA*), com el de Perdew-Burke-Ernzerhof revisat (*revPBE*) i el Armiento-Mattsson (*AM05*). Seguidament, s'ha analitzat el recent meta-GGA fortament lligat i degudament normalitzat (*Strongly Constrained Appropriately Normed – SCAN*). Per últim, també el funcional d'estimació del error bayesià (*Bayesian Error Estimation Functional – BEEF*), obtingut aplicant intel·ligència artificial mitjançant aprenentatge automàtic per ajustar el *xc* a un gran recull de dades experimentals.

Els resultats obtinguts per 27 del TMs en diferents estructures cristal·logràfiques —cúbiques centrades al cos i les cares, i l'hexagonal compacte—, mostren que cap dels funcionals és millor que el Vega-Viñes (*VV*), encara que l'exactitud del SCAN és acceptable, però no pas el BEEF. Al tenir en compte les propietats de 81 superfícies amb índex de Miller més baixos, el resultat és el mateix, sense millorar els resultats del VV per a sòlids (*Vvsol*).

Paraules clau: Teoria del funcional de densitat, Funcionals de bescanvi i correlació, Metalls de transició, Propietats de *bulk,* Propietats superficials, Exactitud.

3. INTRODUCTION

During the last decades, Density Functional Theory (*DFT*) has bloomed as the method of choice in describing diverse chemical systems, from molecules to solid-state materials, simply implying that a given chemical system energy is defined by the electron density function. However, DFT, even if theoretically well formulated, misses a key ingredient, the so-called exchange-correlation (*xc*) functional, which, unfortunately, still has to be approximated. Since the very initial approaches within the Local Density Functional (*LDA*), such as the Ceperley-Alder (*CA*) *xc* functional developed in 1980,[1] dozens of functionals have appeared, mostly aimed at targeting the universal *xc* functional, which would allow describing any type of system and property.

The *xc* functionals are normally classified according to the Jacob's ladder of *xc* functionals improvement,[2] where the lowest rung is represented by LDA *xc* functionals, and higher rungs add accuracy and complexity, up to the top, a heavenly region where the exact *xc* exists, see Figure 1. Initial studies focused at adding rungs above LDA. For instance, LDA works with the electron density, but Generalized Gradient Approximation (*GGA*) adds into account the electron density gradient, and even meta-GGA includes the electron density second derivative. Finally, hybrid functionals add a portion of Hartree-Fock (*HF*) exchange to the *xc* functional; and even higher rungs could be claimed, where the Exact Exchange (*EXX*) is analytically solved.[3]

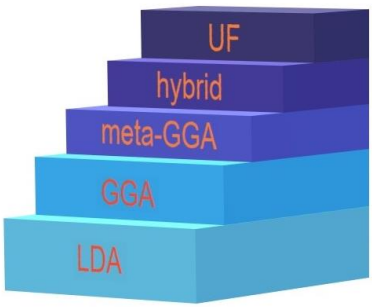

Figure 1. Jacob's Ladder representation of *xc* improvement.

So far the collection of functionals that have been developed fulfilled the Jacob's Ladder dream, particularly as the thermochemistry of main group elements molecules is concerned. However, most recent advances do not necessarily imply a better general description. For instance, it was shown in 2017 that the persistence of researchers on better describing the energetics caused a stray deviation from the path, impoverishing the description of the electron density.[4] Furthermore, the levelling up through Jacob's Ladder does not necessarily imply a better description, as seen *e.g.* on Transition Metals (*TMs*), where extensive studies on 30 TMs bulk and surface properties revealed that GGA level is better suited than higher rank *xc* functionals,[5-7] where the Perdew-Burke-Ernzerhof (PBE) *xc* functional[8] has been found to be the most accurate over 15 different explored *xc* functionals from the first four rungs of Jacob's Ladder for bulk properties,[5,6] and its pole position kept when describing surface properties.[7]

These previous studies aimed at assessing the different DFT *xc flavours* when describing TM systems, but from a broader perspective; this is, evaluating different bulk and surface properties, at variance with the usual approach taken in *xc* development, where frequently only a single property is targeted, *i.e.* the bulk shortest interatomic distance, δ, and normally considering few TM systems, normally late TMs, *e.g.* Pd, Pt, Au, simply because such late TMs are the ones mostly studied and used as heterogeneous catalysts.[9] As one could simply guess, the validation on a single property, on a narrow data set, may lead to large deviations and errors, and this is exactly what was observed for many *xc* functionals.[5-7]

Recent advances in the description of TM systems departed from PBE and implied the adjustment of exchange and correlation coefficients, as in Vega-Viñes (*VV*), or the recovery of the Linear Spin Density (*LSD*) in VV for solids (*Vvsol*).[10] As far as theoretical constrains are concerned, the Strongly Constrained and Appropriately Normed (SCAN) meta-GGA *xc* functional was recently developed so as to meet the 17 theoretical conditions a meta-GGA *xc* must fulfil, and tested for different systems and properties.[11] However, as far as solids were concerned, the evaluation was done only on the lattice constant property, taken from a previous set containing 20 solids, from which there were only for TMs; Cu, Rh, Pd, and Ag, and so, again, being all late TMs, and all displaying a face-centred cubic (*fcc*) crystal structure.[12] A question immediately arises here, in whether such for TMs and a single property were enough to assess the *xc* accuracy for TMs, or whether deviations would arise when using earlier TMs, other bulk properties, or TMs with different crystallographic structures.

Further than that, newer *xc* functionals have been developed with the advent of Artificial Intelligence (*AI*). In this particular aspect, the Bayesian Error Estimation Functional (*BEEF*) used Machine Learning (*ML*) algorithms to adjust it to a plethora of experimental data, including datasets of molecular formation and reaction energies, molecular reaction barriers, non-covalent interactions such as van der Waals (*vdW*) —for what is called sometimes BEEF-vdW—, and bulks lattice constants, cohesive energies, and chemisorption energies on solid surfaces. These datasets included *ca.* 14 TMs, and regarded different properties. Therefore, one would expect a better overall description of BEEF, yet again body-centred cubic (*bcc*) and hexagonal close-packed (*hcp*) TM crystal structures were severely underrepresented, and so, a more complete evaluation should include them in the *proof of the pudding* as done previously for other *xc*.[5-7]

Thus, the present study aims at evaluating the new SCAN and BEEF *xc* functionals in describing three different bulk properties, the shortest interatomic distance, δ, the cohesive energy, E_{coh}, and the bulk modulus, B_0, for 27 TMs featuring *fcc*, *hcp*, or *bcc* crystal structures, see Figure 2. Aside, other earlier functionals are considered, including the LDA parameterization of Hendin-Lundqvist (HL)[13] for the *xc* potential, and the CA parameterization of the electron-gas correlation energy as done by Perdew-Zunger (*PZ*),[14] plus two GGA functionals, the Armiento-Mattsson (AM05), originally designed for the better description of surfaces, yet only tested on Pt,[15] and the revised version of PBE (*revPBE*),[16] argued to better describe the adsorption of atoms and molecules on solid surfaces. For the studied *xc* functional displaying the best overall accuracy, different surface properties, including surface energies, γ, work functions, ϕ, and surface relaxations, Δ_{ij}, have been gained and compared to other *xc* similarly assessed in the literature.[7,10]

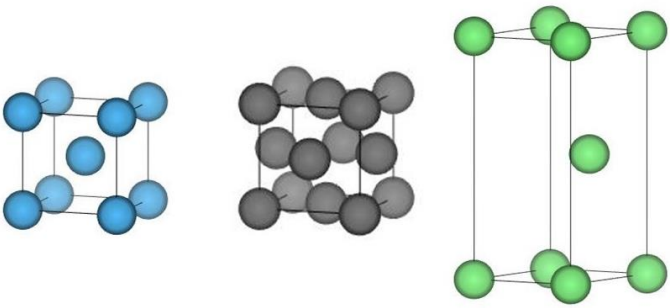

Figure 2. The different studied crystallographic structures, including *bcc* (left), *fcc* (middle), and *hcp* (right). Coloured spheres denote atomic positions.

4. OBJECTIVES

The main objective of the present study is to assess the accuracy of newly developed *xc* functionals in describing a series of bulk properties –δ, E_{coh}, and B_0– for 27 TM bulks in different crystalline structures –*bcc*, *fcc* and *hcp*–, and compare their performance to previously developed *xc* functionals, tested in the literature. In particular, meta-GGA SCAN and ML BEEF GGA will be put a stakes, although other *xc* functionals will be studied, previously not considered, including LDA HL and PZ, and GGA AM05. Most promising and accurate *xc* functionals will be investigated in a second step analysing a series of surface properties –γ, ϕ and Δ_{ij}– on 81 surface models.

Towards this end, the specific objectives could be broken so as to;

- Optimize the bulk structures of the 27 TMs with the six different *xc*, and inspect whether the results are coherent, or whether optimization problems arise.
- Measure the shortest interatomic distance, δ, on the optimized bulk structures, and gain estimates of the cohesive energies, E_{coh}, and bulk moduli, B_0. Such values are used to seize *xc* accuracy by comparing to experimental values, qualitatively detecting systematic errors, and quantitatively estimating the degree of accuracy.
- Interpret the errors and the over- or underestimation with the description of bond strengths, and analyse results with previous studies on the other *xc* functionals, so as to detect global behaviours of LDA, GGA, or meta-GGA *xc* types.
- Ascertain whether SCAN, fulfilling all *xc* conditions, represents an improvement over other meta-GGA *xc* functionals.
- Evaluate whether machine-learned *xc* functionals such as BEEF are a correct path to follow in *xc* development.
- Investigate whether bulk errors are transferable to surface properties by acquiring surface energies, work functions, and interlayer distances, comparing to experimental values and previously investigated *xc* functionals.

5. THEORY

5.1. Schrödinger Equation

The time-independent resolution of the Schrödinger equation is the basis of the Quantum Chemistry discipline, expressed in the well-known equation;

$$\hat{H}\Psi = E\Psi \quad \text{(Eq. 1)},$$

where $\hat{H}$ is the Hamiltonian operator that acts on the chemical system polyelectronic wavefunction, Ψ, so that the operation yields Ψ times the system energy, *E*.

Thus, to solve the equation, one requires to knowing both the wavefunction and the Hamiltonian operator. The latter includes all energetic contributions of nuclei and electrons that configure the system, so that;

$$\hat{H} = \hat{T}_e + \hat{T}_n + \hat{V}_{nn} + \hat{V}_{ee} + \hat{V}_{ne} \quad \text{(Eq. 2)},$$

including the kinetic operators, $\hat{T}$, of nuclei, $\hat{T}_n$ and electrons, $\hat{T}_e$, and the coulombic interaction among nuclei, $\hat{V}_{nn}$, electrons, $\hat{V}_{ee}$, and among nuclei and electrons, $\hat{V}_{ne}$. The problem that prevents exactly solving the equation is this last part, *i.e.* the attraction between electrons and nuclei. A standard approximation to solve the equation was introduced by Born-Oppenheimer (*BO*), noticing that nuclei mass is much larger than that of electrons. Thus, one can decouple the nuclei and electrons movement, and fix the nuclei positions so as to use the so-called electronic Hamiltonian. Within BO approach, the $\hat{T}_n$ is null, and $\hat{V}_{nn}$ a constant.

Still, one requires defining the wavefunction, which is optimized minimizing the system energy through different methods, including HF, Coupled Cluster (*CC*), Configurations Interaction (*CI*), etc. Yet, one of the main problems of Ψ-based methods is the correct description of the electron correlation, targeted in the aforementioned methodologies, but at a high computational time toll. This drawback is circumvented when using DFT, described in the next section.

5.2. Density Functional Theory

The DFT bases in that the electronic density functional of a polyelectronic system describes its energy in the fundamental, ground state. A positive and appealing aspect is that this functional depends only on three spatial coordinates —four when counting spin— instead of three —or four when one counts spin— times the number of electrons and nuclei of Ψ-based methods. This point is key in the computational cost of relatively large systems.

As stated, DFT deals with the electron density, $\rho(r)$, which indicates the probability of finding an electron in a certain volume, and can be mathematically expressed as.

$$\rho(r) = N \int \dots \int |\Psi(x_1, x_2, \dots, x_N)|^2 dx_1, dx_2, \dots, dx_N \qquad \text{(Eq. 3)},$$

for a system containing N electrons. For this, it must comply with the fact that its integral through all the space must result in the number of electrons in the system N; furthermore at infinite distances the integral must cancel out.

$$\int \rho(r) dr = N \qquad \rho(r \to \infty) = 0 \qquad \text{(Eq.4)}.$$

The basis of the DFT relies on two theorems as postulated by Hohenberg and Kohn[17] and an optimization formalism as defined by Kohn and Sham,[18] explained in the following sections.

5.2.1. First Hohenberg and Kohn Theorem

The first Hohenberg and Kohn theorem, also named HK1, states that the electron density the ground state, E_0, can be derived from an external potential, $V_{ext}(r)$, *i.e.* the coulombic field generated by the positive charges of the nuclei at their positions. This indicates that energy can be described as a function of the electron density function, in other words, a functional.

$$E_0 = E_0[\rho(r)] \qquad \text{(Eq. 5)}.$$

Indeed, a reverse mapping is possible, connecting electron density and external potential;

$$\rho(r) \Rightarrow V_{ext}(r) \quad ; \quad V_{ext}(r) \Rightarrow \rho(r) \qquad \text{(Eq. 6)}.$$

This theorem can be proved by a reduction *ad absurdum*, where two different external potentials are sought to define the same electron density, resulting in non-logical statements, although a better, detailed explanation can be found in the literature.[17]

5.2.2. Second Hohenberg and Kohn Theorem

The second Hohenberg-Kohn theorem, also known as HK2, states that the energy of a ground state can be obtained through a variational method. Furthermore, the correct external potential is defined by effect of the exact electron density of the non-degenerate ground state, which is the density that minimizes the total energy. That is, when one has the electron density of the ground state, $\rho_0(r)$, one gains the exact energy of the ground state, E_0. Otherwise, *i.e.* using any other different $\rho(r)$, one gains an energy higher than ground state:

$$E_0 \leq E[\rho(r)] \quad \text{(Eq. 7).}$$

Briefly, as a result of both HK theorems, one can develop a density functional, which can be divided into two parts; the first consisting of the interaction between the external potential and the electron density, and a second term which would be a universal functional, $F[\rho(r)]$. This universal functional does not depends on the system geometry, and can be expressed as the sum of the electrons kinetic energy, $T[\rho(r)$, and the exchange-correlation energetic contributions, $V_{ee}[\rho(r)]$.

If we consider the definition of the universal functional, on a simplified notation, like:

$$F[\rho] \equiv V_{ext}(r) + T[\rho] \quad \text{(Eq. 8).}$$

The equation that defines de electron density functional becomes:

$$E[\rho(r)] = \int \rho(r) V_{ext}(r)\, dr + V_{ee}[\rho] + T[\rho] \quad \text{(Eq. 9).}$$

5.2.3. Kohn-Shan Method

The Kohn-Sham (*KS*) formalism to minimize the energy requires the use of a polyelectronic system of non-interacting electrons with the same density, $\rho(r)$, that the real system under study. Thus, $\rho(r)$ in the reference system can be expressed as the sum of the squares of the Kohn-Shan orbitals, $\phi_i(r)$,[19] plus the kinetic energy of the electrons is treated as if electrons do not interact with each other:

$$\rho(r) = \rho_{KS}(r) = \sum_{i=1}^{N} |\phi_i(r)|^2 \quad \text{(Eq. 10),}$$

$$T_s[\rho] = \sum_{i=1}^{N} \langle \phi_i \left| -\frac{1}{2}\nabla^2 \right| \phi_i \rangle \quad \text{(Eq. 11).}$$

Thus, it is possible minimize the real system energy using the reference system of non-interacting electrons, so that the functional ends being formulated, in a simplified fashion, more simplified, as:

$$E \equiv T_s + E_{ext} + J + E_{xc} \quad \text{(Eq. 12),}$$

where T_s is the kinetic energy of electrons, E_{ext} the attraction between the external potential and the electron density, J the Coulomb repulsion between electrons, and, finally, E_{xc} is a functional that includes the exchange and correlation energies, in addition to the energy difference between the real and reference system. The main hurdle of DFT is in this last term, whose universal expression is not known, and contains all the energy contributions that do not have a simple dependence on the electronic density:

$$E_{xc}[\rho] \equiv T[\rho] - T_s[\rho] + V_{ee}[\rho] - J[\rho] \qquad \text{(Eq. 13)}.$$

Despite of the many attempts, explained in the next section, the universal expression of E_{xc} is still missing, and so, DFT may remain accurate, yet not exact. In the next section the many types of developed *xc* functionals are summarized, emphasizing those under scrutiny in the present study.

5.3. Exchange and Correlation Functionals

As introduced in the previous section, the KS formalism requires an approximated *xc* functional, and, as commented in the Introduction, nowadays there are only approximations, classified in accordance to their complexity in the Jacob´s Ladder, as shown in Figure 1. In the next subsections we briefly introduce the main three rungs, and the functionals explored within.

5.3.1. Local Density Approximation

The simplest way to account for the exchange and correlation energy corresponds to the first rung on Jacob's Ladder, this is, the local density approximation. Within LDA, one considers the electron density equal to that of an ideal and uniform electron gas system, called Jellium, where the exchange and correlation functional is known. Within this system, the electron density gradients are approximately zero, and from this its follows that the exchange and correlation potentials can be separated;

$$E_{xc}^{LDA}[\rho] = E_x[\rho] + E_c[\rho] \qquad \text{(Eq. 14)}.$$

The LDA *xc* functionals are thought to be good for systems with slow decaying electron densities, such as metals. However, LDA *xc* functionals are known to overestimate bonds, and should not be used to describe strongly correlated systems.

The fist *xc* functional that have been studied within LDA rung is the Hendin-Lundqvist.[13] The HL *xc* functional based on advancements of the electron gas interaction theory. It provided numerical data for the effective *xc* potentials of the ground state and exited states. The *xc* functional consisted of exposing the *xc* potential as a factor that depends on the local density.

This factor, called *p*, varies between 1-1.5 depending on whether the density is high, $p = 1$, or low, $p = 1.5$. This analytical approach is mapped linearly, and this *xc* functional was found suitable for valence electrons and for ionic where nuclei are treated separately.[13]

The second studied *xc* functional of this rung is the Perdew-Zunger.[14] This PZ *xc* functional parametrized the electron-gas correlation energy at any density, numerically adjusting to the exchange-correlation hole. In addition, it made a correction of the potential of a self-consistent electron through the variational method. Furthermore, it was claimed to be adequate to mitigate the self-interaction energy. Consequently, it was stated to provide an improvement for the total energy as a result of treating the exchange and correlation separately.[14]

5.3.2. Generalized Gradient Approximation

In the second rung of the Jacob's Ladder, the GGA, one introduces the density gradient or density variations with position, in addition to the dependencies already contained in LDA. Thus, the GGA *xc* depend not only on $\rho(r)$, but in its gradient, $\nabla\rho(r)$;

$$E_{xc}^{GGA}[\rho(r)] = \int f(\rho(r), \nabla\rho(r))dr \qquad \text{(Eq. 15)}.$$

Here the revised Perdew-Burke-Ernzerhof (revPBE) GGA *xc* was considered.[16] This *xc* functional is alleged to improve some deficiencies of PBE, for instance, making variable the local rotation density. Furthermore, it was alleged to provide improvements in the molecular atomization energies and atomic total energies,[16] and it is also known to deliver better adsorption energies.

Secondly, the Armiento-Mattsson (AM05) *xc* functional is also explored.[15] This functional was claimed to deliver a precise treatment of the system for electronic surfaces. For this, two functional parts are combined, one aimed for surfaces and another for internal areas. Consequently, AM05 was advised for solid state studies, *e.g.* when describing bulk properties and surface properties.[15]

Finally, the Bayesian error estimation functional is studied. This BEEF *xc* functional is one of the major successes in the last years because it is said to have a great applicability to complex surface study systems. The approximations of this *xc* functional and its estimation of Bayesian error mark the difference with the rest of the *xc* functionals. As already mentioned in the introduction, it is characterised by using ML protocols in its outline, and by having very good transferability.[20]

5.3.3. Meta-GGA

When the kinetic energy or Laplacian density is added, a third rung of Jacob's Ladder is climbed, the so-called meta-GGA, which, in other words, include the second derivative of the electron density in the *xc* formula *ansatz*. The only *xc* functional tested in this study is the strongly constrained appropriately normed one.[11] The SCAN *xc* has been found to be a very accurate meta-GGA for systems where the exchange-correlation hole is located close to the electron because it gets strongly restricted and adequately normalized. More than that, this *xc* functional is characterized by complying with each of the 17 restrictions a *xc* functional must have. In addition, for unbound interactions and gases it is said to very precisely comply with the appropriate standards. Thus, the SCAN *xc* functional is good for lattice constants and weak interactions.[11]

5.3.4. Higher rungs

The fourth rung of Jacob's Ladder normally relates to hybrid functionals, which are linear combinations of LDA, GGA, or meta-GGA *xc* functionals, but always adding a portion of the HF exchange. Examples of them are PBE0,[21] range-separated HSE06,[22] or the popular B3LYP,[23] extendedly used in molecular thermochemistry. However, hybrid functionals are known to poorly describe metal systems, as tend to localize the electron density.[24] However, hybrid functionals may well be suited in describing semiconductor materials.[24] Upper than that, there would be the EXX xc,[3] which, formally, is correct, but its accuracy is handicapped by a very high computational costs, so that its practical use nowadays has restricted to particular cases as proof-concepts.

5.4. Bulk Description

Most of the condensed phases of matter display a crystallographic structure with an intrinsic periodicity. Thus, they can be described with a periodic model instead of an aggregate or cluster model, necessary for amorphous materials. Within the periodic model the solids are ordered under Periodic Boundary Conditions (*PBC*) conditions, which greatly simplifies their description, as one basically requires a small portion of the solid, the so-called unit cell, that is infinitely translationally repeated to model the macroscopic solid.

Any unit cell is defined by three vectors, $\vec{a}$, $\vec{b}$, and $\vec{c}$, and the angles between them. Along the three vectors one can apply integer replications, on which the translational operator, $\hat{T}$, is built. This periodic pattern is called a crystalline lattice or Bravais lattice.

$$\hat{T} = n_1\vec{a} + n_1\vec{b} + n_1\vec{c} \qquad \text{(Eq. 16).}$$

The crystal lattice is finally formed by combining the vectors of the unit cell with the atomic base, *i.e.* the atomic positions which are translationally replicated. In this work we will focus on the most common crystal structures of TMs, being *bcc* for V, Cr, Fe, Nb, Mo, Ta, W, *fcc* for Ni, Cu, Rh, Pd, Ag, Ir, Pt, and Au, and *hcp* for Sc, Ti, Co, Y, Zr, Tc, Ru, Hf Re, and Os. This accounts for 27 out of 30 TMs, excluding La, which displays a simple hexagonal unit cell, Mn, featuring a *bcc* crystal structure but with an atomic based composed of Mn_{29} clusters, and Hg, which is liquid under normal working conditions. This way, one could analyse the results as a function of the crystallographic structure with enough data so as to carry a proper statistical analysis.

5.4.1. The Bloch Theorem

When transferring the unit cell from a point r to an equivalent point of a replicated cell $r + R$ applying the translation operator, $\hat{T}$, one should get the same wavefunction except for a change phase.

$$\hat{T}\Psi = \Psi(r + R) = \Psi(r) \qquad \text{(Eq. 17).}$$

As above explained, the external potential, $V_{ext}(r)$, determines the electron density within the unit cell and causes the wavefunction to be unaffected in moving from one point to an other equivalent one, and, therefore, its properties are treated periodic as well.

Bloch theorem states that in a periodic system, like the ones addressed in this study, each wavefunction of the real system can be expressed as a sum of plane waves defined by the **G** vector in the reciprocal space. Considering that each planewave with wavevector **k** is characterized by a kinetic energy, a finite base of plane waves can be constructed defining a limit for its kinetic energy.

$$\Psi_i = \sum_G c_{i,k+G} e^{i(k+G)r} \qquad \text{(Eq. 18).}$$

The lattice vectors for the reciprocal space that is used to define the wavevectors **k** results form the real space lattice, **a**, **b**, **c**, and constructed orthogonal to them. A key feature of this reciprocal space is that the lattice vector length is inversely proportional to its real counterpart; *i.e.* a large real vector yields a short reciprocal vector, and *vice versa*. The lattice vectors for the reciprocal space, b_a, b_b, and b_c, are connected to the real space lattice vectors, a_a, a_b, and a_c like:

$$b_a = 2\pi \frac{a_b \times a_c}{a_c \times (a_b \times a_c)} \; \forall_{a,b,c} \in \{1,2,3\} \quad \text{(Eq. 19).}$$

$$a_a \times b_b = 2\pi \delta_{ab} \quad \text{(Eq. 20).}$$

5.5. Bulk Properties

Different bulk properties are investigated so to assess the *xc* performance while comparing to the experimental values. These are the interatomic distances, δ, the cohesive energy, E_{coh}, and the bulk modulus, B_0, explained next.

5.5.1. Interatomic Distances

The first studied property is quite simple; this is the shortest interatomic distance between neighbouring metal atoms within the bulk unit cell, δ. At variance with other works, the lattice parameter has not been used, as the unit cell is an arbitrary construct, and so the lattice vectors lengths, making it less fair a comparison, particularly when willing to mix results from different crystallographic structures. Consequently, the comparison on the shortest interatomic distance is a better playground, as is not affected by neither cell definitions nor crystallographic preferences.

5.5.2. Cohesive Energy

The cohesive energy, E_{coh}, can be defined as the energy needed to disaggregate the bulk atoms into isolated atoms in the vacuum. From another perspective, it could be seen as the freed energy when such isolated atoms coalesce into a bulk. To estimate the cohesive energies, one could use the following expression;

$$E_{coh} = E_{at} - \frac{E_{bulk}}{N} \quad \text{(Eq. 21),}$$

where E_{at} is the energy of an atom isolated in the vacuum, and E_{bulk} the energy of a bulk material containing N atoms. This defined, the more positive the E_{coh} is, the stronger the bonds in the bulk are.

5.5.3. Bulk Modulus

The bulk modulus, B_0, defines the compression or expansion capacity of the bulk, defined as

$$B_0 = -V_0 \left(\frac{\partial P}{\partial V}\right)_T \quad \text{(Eq. 22),}$$

where V_0 is the unit cell volume at the ground state, and changes are applied depending on pressure, P, at a fixed temperature, T. For instance, a large B_0 implies a small volume change with a great pressure, *i.e.* difficult to be compressed/expanded. The B_0 values are acquired by

single point calculations varying the volume near V_0, and adjusting the trend to a line to gain the slope.

5.6. Surface Description

In order to model solid surfaces under PBC conditions, it is extended to use slab models. Such models consist of increasing the unit cell in the direction of the considered plane. These planes are described using the Miller indices, defined by the lattice vectors of the reciprocal normal to the plane ($\vec{h},\vec{k},\vec{l}$), and normally noted (*hkl*). Usually the most stable surfaces are those with lower Miller indices, and so, the explored surface for *fcc* and *bcc* crystallographic structures are the (001), (011) and (111) ones. For TMs with hexagonal *hcp* structures, the most stable planes are the (0001), ($10\bar{1}0$), and ($11\bar{2}0$). In such hexagonal structures, a fourth index is used; (*hkil*), where *j = - (h + k)*, and used for practically, so as to deal with orthogonal vectors.

As above stated, a vacuum is created normal to the surface direction to avoid interactions between translationally repeated slabs. Usually, 10 Å of vacuum is enough to prevent such. Furthermore, a slab model requires having zones modelling both the bulk and the surface. This can be achieved by imposing a certain number of atomic layers, with two possibilities; either a symmetric slab, in which two surfaces are exposed, and the inner layer model the material bulk, or an asymmetric slab, where one half of the slab is optimized, modelling surface, while the other half is kept at bulk positions, modelling the material interior. In the present work, symmetric slabs where all atomic layers were allowed to relax were used.

5.7. Surface Properties

Similarly to bulk, different energetic, structural, and electronic properties are investigated. In particular, and following a previous work,[7] we explored surface energies, γ, work functions, ϕ, and the interlayer distance relaxation, Δ_{ij}, briefly explained next.

5.7.1. Surface Energy

The surface energy, γ, is the most characteristic feature of surfaces, which are the natural defects of an otherwise infinite crystal. They can be through as the energetic cost of separating the bulk by a plane, given per surface area. Estimates of γ can be gained using de following formula:

$$\gamma = \frac{E_{slab} - (N \cdot E_{bulk})}{2A} \quad \text{(Eq. 23),}$$

where E_{slab} is the slab total energy composed of N atoms, E_{bulk}, the total energy of an atom in bulk environment, and *A* is the surface area of each one of the two equivalent exposed surfaces within the slab model.

5.7.2. Work Function

The work function, ϕ, refers to the energetic cost of moving an electron from the Fermi level, E_F, and place it into to the vacuum energy level, *V*, as:

$$\phi = V - E_F \qquad \text{(Eq. 24).}$$

This work function is normally related to the photoelectric effect, and related to diverse features, such as the redox capabilities of the studied surfaces.

5.7.3. Interlayer Distances

The interlayer distance is simply a measure the distance between the atoms of the slab that are in the contiguous layers. For this, a percentage relation of the contraction/expansion of the surface is used, Δ_{ij}.

$$\Delta_{ij} = \left(\frac{\delta_{ij} - \delta_{ij}^{bulk}}{\delta_{ij}^{bulk}} \right) \cdot 100 \qquad \text{(Eq. 25).}$$

Where δ_{ij} is the interlayer distance, *i.e.* δ_{12} is the distance between the surface layer and the fist surface layer, and δ_{23} the distance between the two first subsurface layers. The δ_{ij}^{bulk} reference value is always a constant, referred to the interlayer distance in bulk environment.

6. COMPUTATIONAL DETAILS

The present DFT calculations have been carried out using the Vienna *Ab Initio* Simulation Package (*VASP*) suite.[25] The computational calculation setup follows that of the earlier study of Janthon *et al.*[5] Briefly, for bulk calculations, optimal Monkhorst-Pack **k**-points grid of 7×7×7 dimensions were used, while for isolated atoms, Γ-point calculations were carried out when isolated in a broken symmetry cell of 9×10×11 Å dimensions. Core electrons were treated using Projector Augmented Wave (*PAW*) pseudopotentials.[26] A plane-wave basis set for the valence electron density was used, with a 415 eV cutoff for the kinetic energy. This ensures having energy estimates converged below the chemical accuracy of ~0.04 eV. The electronic convergence criteria was always set to 10^{-6} eV and relaxations on atoms stopped when having differences in energies in consecutive structures below 10^{-5} eV.

The electronic structure calculations were not spin polarized, with the exception of the calculations on the ferromagnetic Fe, Ni, and Co bulk systems, their surfaces, and of any isolated metal atom. Optimizations were performed using the tetrahedron smearing method of Blöchl *et al.*[27] with an energy width of 0.2 eV to speed up convergence, yet final energies were extrapolated to zero smearing. For B_0 calculations, the optimized bulk was enlarged/contracted by ±0.05 and ±0.10 Å variations of the lattice constants. Notice that CA PAW pseudopotentials were used when testing LDA HL and PZ *xc* functionals,[13,14] whereas PBE PAW pseudopotentials were used for the revPBE, AM05, SCAN, and BEEF *xc* functionals.[11,15,16,20] The bulk[5] and surface[7] models were obtained and adapted from previous works, and further details about them can be found in the literature.

7. RESULTS AND DISCUSSION

7.1. Bulk Properties *xc* Performance

Firstly, the 27 TMs bulks were optimized using the six explored *xc* functionals, these are, the HL and PZ LDA types, the GGA ones revPBE, AM05, and BEEF, and the SCAN meta-GGA, accounting for a total number of 162 structural bulk optimizations. The computed interatomic distances are listed in Table 1, while the cohesive energies and bulk moduli are encompassed in Tables 2 and 3, respectively. Such computed values are compared to available experimental data in the literature,[5] duly temperature corrected for a fairer comparison with our zero Kelvin estimates. For a better statistic analysis, we computed mean errors, in particular the Mean Error (*ME*), the Mean Absolute Error (*MAE*), and the Mean Absolute Percentage Error (*MAPE*).

These errors are shown in Table 4, and there one can readily observe that shortest interatomic distances have the smallest errors with respect experimental values, differing, in absolute terms, by 0.05 Å (AM05) to 0.13 Å (BEEF). When having a look to the signed ME, we see that no systematic error is found in general, as normally over- and underestimated values compensate, except for revPBE, which systematically delivers larger distances than in experiments, similar to the RPBE.[6] The *xc* functional that presents the best results for δ is AM05, while the worst is BEEF. In any case, the errors for δ are quite small, raging 2.5 to 4.5% in MAPE, with no clear difference in performances of LDA, GGA, or meta-GGA approximations.

As far as the cohesive energy errors are concerned, still the best *xc* is the AM05, with a MAE of only 0.51 eV, although revPBE or SCAN are technically equal, with MAEs of 0.59 and 0.55 eV, respectively. Thus, GGA or meta-GGA levels seem suited in describing E_{coh}, and LDA *xc* types, or even BEEF, should not be advised. Particularly, the BEEF results are again the worst case, with a large MAE deviation of 1.34 eV. Further than that, some *xc* provide systematic errors, as observed *e.g.* on HL, which systematically overestimates the E_{coh} values, and so almost happens with PZ *xc* functional. This is known to be typical for LDA *xc* functionals, which overestimate the bonding strengths.[5]

TM	Structure	HL	PZ	revPBE	AM05	SCAN	BEEF	EXP.
Sc	*hcp*	3.118	3.116	3.285	3.179	3.264	2.949	3.244
Ti	*hcp*	2.818	2.816	2.904	2.851	2.866	2.916	2.889
V	*bcc*	2.534	2.532	2.604	2.557	2.579	2.620	2.606
Cr	*bcc*	2.420	2.419	2.479	2.438	2.448	2.496	2.485
Fe	*bcc*	2.387	2.387	2.466	2.409	2.377	2.518	2.450
Co	*hcp*	2.408	2.404	2.487	2.431	2.404	2.518	2.488
Ni	*fcc*	2.424	2.420	2.508	2.445	2.421	2.545	2.484
Cu	*fcc*	2.495	2.494	2.590	2.521	2.545	2.642	2.544
Zn	*hcp*	2.785	2.788	2.928	2.814	2.880	3.081	2.645
Y	*hcp*	3.444	3.443	3.614	3.502	3.592	3.443	3.548
Zr	*hcp*	3.146	3.144	3.219	3.167	3.186	3.149	3.174
Nb	*bcc*	2.826	2.825	2.887	2.841	2.857	2.912	2.854
Mo	*bcc*	2.701	2.709	2.757	2.718	2.735	2.779	2.721
Tc	*hcp*	2.690	2.689	2.738	2.698	2.700	2.766	2.705
Ru	*hcp*	2.616	2.615	2.667	2.625	2.621	2.697	2.642
Rh	*fcc*	2.664	2.663	2.729	2.677	2.672	2.777	2.532
Pd	*fcc*	2.725	2.726	2.813	2.745	2.809	2.880	2.745
Ag	*fcc*	2.892	2.838	2.974	2.880	2.890	3.071	2.877
Cd	*hcp*	3.207	3.207	3.369	3.255	3.282	3.571	2.959
Hf	*hcp*	3.058	3.056	3.158	3.097	3.065	3.176	3.126
Ta	*bcc*	2.822	2.820	2.888	2.840	2.826	2.907	2.856
W	*bcc*	2.726	2.725	2.772	2.735	2.726	2.790	2.738
Re	*hcp*	2.722	2.722	2.762	2.726	2.733	2.777	2.564
Os	*hcp*	2.658	2.657	2.701	2.665	2.647	2.720	2.671
Ir	*fcc*	2.701	2.700	2.749	2.706	2.705	2.781	2.710
Pt	*fcc*	2.762	2.762	2.823	2.769	2.732	2.876	2.766
Au	*fcc*	2.874	2.872	2.973	2.895	2.915	3.072	2.870

Table 1. Calculated and experimental shortest interatomic distances, δ, given in Å, for the studied bulk TMs, and the experimental values, corrected for zero-point energy and finite temperature effects from Lejaeghere *et al.*[28]

Notice as well that the E_{coh} displays much larger MAPE errors, going from *ca*. 10% to 30%. This, compared to the δ MAPE errors of 1-5%, already evidences that *i)* such functionals were, mainly, tailored to reproduce bond distances and lattice parameters, thus begin more accurate, and, accordingly, displaying smaller errors, and *ii)* that this may lead to a poorer description of other properties, like energetics, here evidenced by E_{coh} MAPE values, or even signifying that such an adjustment may implicitly lead to a stray deviation of other properties, like energetics, here evidenced by E_{coh} MAPE values, or even signifying that such an adjustment may implicitly lead to a stray derivation of other properties, as observed, *e.g*. in electron densities.

This is also observed when inspecting bulk moduli, as the MAPE values range 10-27%, see Table 4. There, the presently studied *xc* functional that best describes the bulk moduli of TMs in average terms studied is the revPBE. The LDA display basically systematic errors overestimating the B_0 by ~40 GPa, which goes along with the aforementioned bond strength overestimation. Notice that, to some extent, AM05 provides similar results, with a systematic overestimation of ~28 GPa. The worst case is again BEEF, with large deviations, as seen with ME and MAE errors of *ca.* -33 and 43 GPa, respectively, and a MAPE close to 26%, which underscores the large dispersion of results.

TM	Structure	HL	PZ	RE	AM	SCAN	BEEF	EXP.
Sc	*hcp*	4.85	4.88	3.79	4.37	4.34	3.16	3.93
Ti	*hcp*	6.69	6.50	5.05	5.92	5.71	4.25	4.88
V	*bcc*	7.25	7.42	4.87	6.42	5.67	4.28	5.34
Cr	*bcc*	6.53	5.65	3.49	4.42	3.99	2.81	4.15
Fe	*bcc*	6.52	6.46	4.34	5.47	5.82	3.49	4.32
Co	*hcp*	6.53	6.50	4.72	5.67	5.68	3.93	4.47
Ni	*fcc*	5.95	6.02	4.28	5.19	4.89	3.56	4.48
Cu	*fcc*	4.47	4.09	3.07	3.76	3.85	2.34	3.51
Zn	*hcp*	1.91	1.37	0.81	1.35	1.32	0.14	1.38
Y	*hcp*	4.85	4.89	3.80	4.39	4.18	4.89	4.42
Zr	*hcp*	7.30	7.38	5.82	6.69	6.16	7.38	6.32
Nb	*bcc*	8.05	8.52	6.42	7.47	6.96	5.64	7.47
Mo	*bcc*	7.55	8.13	5.63	6.80	5.70	7.86	6.84
Tc	*hcp*	8.50	8.84	6.20	7.61	6.97	5.10	7.17
Ru	*hcp*	8.54	8.77	6.03	7.52	7.76	4.82	6.80
Rh	*fcc*	7.54	7.54	5.30	6.39	6.46	4.20	5.76
Pd	*fcc*	5.03	5.03	3.19	4.10	4.16	2.22	3.93
Ag	*fcc*	3.56	2.96	2.05	2.73	2.72	2.75	2.96
Cd	*hcp*	1.55	1.52	0.42	0.83	0.91	-0.16	1.18
Hf	*hcp*	7.48	7.56	5.98	6.88	6.65	5.08	6.44
Ta	*bcc*	9.56	9.65	7.74	8.86	8.79	6.68	8.11
W	*bcc*	10.39	10.61	8.40	8.78	9.65	7.19	8.83
Re	*hcp*	9.43	9.76	8.75	8.52	8.32	5.88	8.06
Os	*hcp*	10.12	10.25	7.69	9.23	9.17	6.26	8.22
Ir	*fcc*	9.18	9.27	6.64	8.12	8.08	5.31	6.96
Pt	*fcc*	6.91	6.94	4.93	6.15	6.36	3.77	5.87
Au	*fcc*	4.24	3.40	2.49	3.33	3.32	1.68	3.83

Table 2. Calculated and experimental cohesive energies, E_{coh}, given in eV/atom, for the studied bulk TMs, and the experimental values, corrected for zero-point energy and finite temperature effects from Lejaeghere *et al.*[28]

TM	Structure	HL	PZ	revPBE	AM05	SCAN	BEEF	EXP.
Sc	*hcp*	62.8	62.0	53.0	57.4	56.6	38.7	55.6
Ti	*hcp*	128.5	128.6	108.5	119.6	115.4	105.0	108.3
V	*bcc*	215.3	216.2	180.8	202.9	174.1	169.9	158.9
Cr	*bcc*	310.6	311.4	257.6	291.3	288.2	241.8	174.5
Fe	*bcc*	270.3	271.7	209.4	238.4	246.6	125.0	169.8
Co	*hcp*	278.3	242.1	205.5	247.7	218.8	177.7	193
Ni	*fcc*	258.1	263.4	182.5	233.3	256.5	153.3	185.5
Cu	*fcc*	114.3	186.0	130.2	165.3	147.4	103.9	140.3
Zn	*hcp*	114.1	113.2	75.9	99.0	102.8	54.2	69.7
Y	*hcp*	44.1	44.1	39.4	41.5	41.8	57.8	41.7
Zr	*hcp*	103.9	104.0	90.7	98.3	96.8	125.0	95.9
Nb	*bcc*	196.1	196.3	170.6	188.1	193.8	106.1	172
Mo	*bcc*	300.7	302.4	259.5	290.7	297.6	236.1	264.7
Tc	*hcp*	351.9	352.5	297.5	349.6	334.7	262.4	303.1
Ru	*hcp*	374.3	374.9	303.7	357.3	375.9	254.1	317.7
Rh	*fcc*	324.2	323.6	244.5	302.0	307.6	194.3	288.7
Pd	*fcc*	229.4	227.5	159.2	204.5	164.5	116.9	195.4
Ag	*fcc*	140.4	140.6	78.0	115.0	88.8	40.7	103.8
Cd	*hcp*	80.5	80.3	45.9	66.4	56.8	7.4	53.8
Hf	*hcp*	108.3	122.5	107.5	114.3	121.0	104.5	109.7
Ta	*bcc*	216.4	220.4	191.2	209.1	204.9	184.5	193.7
W	*bcc*	345.9	346.3	304.9	336.1	332.1	332.6	312.3
Re	*hcp*	420.7	421.5	371.9	415.7	374.6	342.0	368.8
Os	*hcp*	458.8	460.6	397.0	453.2	479.4	351.4	424.6
Ir	*fcc*	411.0	411.7	340.0	398.7	407.4	282.4	365.2
Pt	*fcc*	310.9	311.6	239.9	295.6	379.2	181.4	284.2
Au	*fcc*	194.4	196.1	125.6	171.6	153.3	78.3	174.8

Table 3. Calculated and experimental bulk moduli, B_0, given in GPa, for the studied bulk TMs, and the experimental values, corrected for zero-point energy and finite temperature effects from Lejaeghere *et al.*[28]

Finally, having analysed the performance depending on each study the property, it would be convenient to get an estimate of the performance in general terms. As we compare different structural, energetic, and elastic properties, there is no direct ground to make such a comparison, so the only viable way of approaching it is by adding up the MAPEs of each property. This is visually shown in Figure 3, revealing that the best suited *xc* would be revPBE, with an added MAPE accuracy of 26.86%, but, one has to honestly state that AM05 and SCAN performance is quite close, with values of 27.47% and 28.7%, respectively.

Error	xc	δ	E_{coh}	B_0
MSE	HL	-0.01	1.29	38.5
	PZ	-0.01	1.27	41.0
	revPBE	0.07	-0.51	-5.8
	AM	0.01	0.42	27.3
	BEEF	0.09	-1.15	-33.3
	SCAN	0.02	0.29	25.6
MAE	HL	0.06	1.29	40.5
	PZ	0.06	1.30	41.0
	revPBE	0.07	0.59	18.1
	AM	0.05	0.51	27.6
	BEEF	0.13	1.34	43.9
	SCAN	0.06	0.55	30.6
MAPE	HL	2.22	25.91	23.7
	PZ	2.28	23.83	24.1
	revPBE	2.63	14.22	10.0
	AM	1.78	10.49	15.2
	SCAN	4.49	29.63	26.1
	BEEF	2.15	10.85	15.7

Table 4. Analysis of the ME, MAE, and MAPE errors of the calculated interatomic distances, δ, in Å, cohesive Energies, E_{coh}, in eV/atom, and the bulk moduli, B_0, in GPa, with respect the experimental values reported in Tables 1-3.

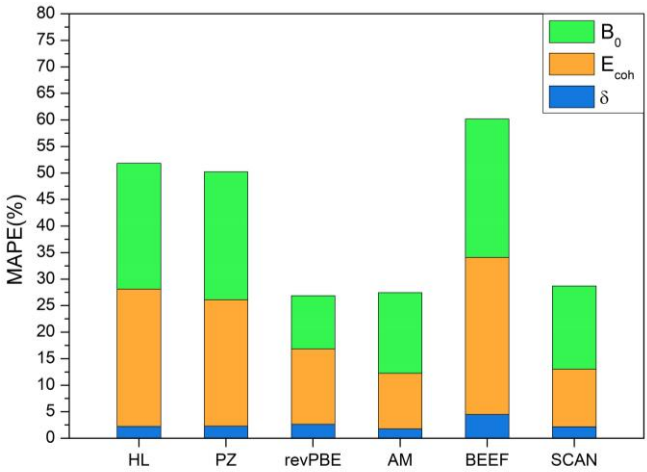

Figure 3. Added MAPEs for the δ, E_{coh}, and B_0, for the different explored *xc*.

Other than that, the results show that LDA should be avoided in the description of bulk TM, and so BEEF, both particularly because do not provide a fairly good description neither for Ecoh nor for bulk moduli, even if Ecoh bulk moduli where used in the xc adjustment. This poor performance may be due to a short data set, or the willingness of describing anything, even when different chemical systems may require different xc functional treatments.

7.2. Results Validity

For most of the studied *xc* functionals, there has not been previous studies like the present one, with one sole exception; Jana *et al.* recently analysed the SCAN performance for all the studied TMs, including as well some alkaline and alkaline-earth metals.[29] Table 5 shows the ME, MAE, and MAPE errors using the same experimental reference for both the present study and the previous work of Jana *et al.*,[29] revealing a fairly good agreement, *i.e* both studies displaying low errors for δ, and large for both E_{coh} and B_0 properties.

Error	Source	δ	E_{coh}	B_0
ME	Present	0.02	0.29	25.6
	Ref. 29	0.01	0.17	18.0
MAE	Present	0.06	0.55	30.6
	Ref. 29	0.04	0.52	24.6
MAPE	Present	2.15	10.85	15.7
	Ref. 29	1.37	10.01	13.7

Table 5. Analysis of the ME, MAE, and MAPE errors for the SCAN *xc* functional, as calculated in the present work or taken from Jana *et al.*[29]

However, these previous calculations featured somewhat lower errors, as can be seen in any property in Table 5. Some of these lower values could be argued to be within chemical accuracy, see differences of solely 0.03 eV/atom for E_{coh}, and excellent match in MAPEs, with differences that are below 2%. We attribute this small, almost negligible differences to small change in the computational setup, for instance, using a larger basis set with a kinetic cutoff energy limit of at least 500 eV for the plane waves, and denser **k**-points grids of 16×16×16 dimensions.

In any case, it is comforting to observe that a denser **k**-point sampling with a better basis set provided more accurate results, although for sure paying a computational cost which we could

not meet in the realization of this project. Regardless of the previous, and in order to compare to previous exhaustive studies carried out as here done, we keep the same computational approach in the previous and oncoming analysis.

7.3. Literature Comparison

Reached this point some questions arise: Is any of the here-studied *xc* functionals the most accurate in describing TM bulks, while regarding the ones already studied in the literature? Are the functionals in the different rungs behaving similarly? To answer these questions, the MAPE errors for the bulk properties of the studied *xc* functionals are compared with other exchange-correlation functionals already tested with the same computational setup. These are the Ceperley-Alder (*CA*),[1] Vosko-Wilk-Nusair (*VWN*),[30] Perdew-Burke-Ernzerhof (*PBE*),[8] Perdew-Burke-Ernzerhof revised for solids (*PBEsol*),[31] and revised Perdew-Burke-Ernzerhof (*RPBE*)[32] functionals, taken from Janthon *et al.,*[6] plus the Tao-Perdew-Staroverov-Scuseria (*TPSS*)[12], revised Tao-Perdew-Staroverov-Scuseria (*revTPSS*)[12], a local density functional M06L,[33] Minnesota 12 (*MN12-L*),[34] the PBE hybrid (*PBE0*),[21] hybrid density functional based on a screened Coulomb potential for the exchange interaction (*HSE06*),[35] and hybrid functional (*B3LYP*)[36] functionals from a posterior study by Janthon *et al.*[5] Last but not least, the VV[10] and VVsol[10] *xc* functionals as adapted in treating TM systems have been accounted. All such values are listed in Table 6 broken down for the δ, E_{coh}, and B_0.

From such values, visually shown in Figure 4, one observes that LDA functionals (HL, PZ, CA, and VWN) are not suited in the description of TMs, as they largely fail in estimating E_{coh} and B_0, a point which puts the spotlight in the fact that while the lattice parameters may depend mostly on the electron density, these other properties do depend on the electron density gradient. This is clearly observable on the GGA *xc* functionals (PBE, PBEsol, RPBE, revPBE, BEEF, VV, and VVsol), which are, by far, while in average terms, the best approximations describing TM bulk properties, being VV the best one reported so far.[10] Finally, the meta-GGA (TPSS, revTPSS, M06-L, MN12-L, and SCAN) are slightly worse in general, where TPSS is perhaps the best one. Finally, the use of hybrid *xc* (PBE0, HSE06, and B3LYP) is detrimental, as provide worse results, due to their tendency in localizing the electron density, which goes against nature concerning the metallic electronic structure.[24]

BEEF deserves a special mention. This machine learned *xc* functional provides errors similar, or even worse, than LDA functionals. Thus, the initiative to correlate different types of

systems and properties by ML means is, apparently, a failure when going out from the studied dataset. This forces to rethink whether the artificial intelligence approach was duly treated: for instance, and whether a larger and more complete training set was necessary, or whether different *xc* functionals should we developed for different families of systems and/or properties.

xc	δ	E_{coh}	B_0	Sum
HL	2.22	25.91	23.68	51.81
PZ	2.28	23.83	24.11	50.22
CA	2.24	27.24	23.75	26.89
VWN	2.38	26,94	27.84	27.48
revPBE	2.63	14.22	10.03	28.73
AM05	1.78	10.49	15.22	60.20
BEEF	4.49	29.63	26.09	20.70
PBE	1.40	10.90	8.40	24.10
PBEsol	1.60	14.16	17.72	30.30
RPBE	1.66	14.49	9.21	27.90
VV	1.84	8.77	8.16	35.30
VVsol	1.33	10.07	11.75	39.40
SCAN	2.15	10.85	15.72	35.00
TPSS	1.40	10.00	12.70	52.80
revTPSS	1.50	11.20	17.60	58.68
M06-L	1.90	10.60	15.40	57.16
MN12-L	2.00	13.70	19.60	33.48
PBE0	1.20	24.00	14.20	25.36
HSE06	1.10	21.70	12.20	18.77
B3LYP	2.20	37.70	12. 90	23.15

Table 6. MAPE errors from different *xc* functionals, here calculated, or taken from literature.[3]

7.4. Surface Properties

After the analysis of the *xc* functionals performance when considering the bulk properties, a missing question was still open; can this bulk properties accuracy be extrapolated to surface properties? To this end, three different surfaces for each metal have been modelled, as previously stated, and for these the surface energies, γ, workfunctions, ϕ, and interlayer distances, δ_{ij}, have been calculated. Given the real and computational time limitations, we focused only on the most promising *xc* functional, this is, the revPBE, which implied 81 more optimizations. The amount of acquired information is quite large, indeed, exceeding the possibilities to report them within the space limit of the present report. Thus, Tables 7 and 8

shows examples of the γ and ϕ values, for the exemplary cases of *bcc* Fe, *fcc* Cu, and *hcp* Ti. As far as interlayer distances are concerned, the Δ_{ij} values are provided, as listed in Table 9.

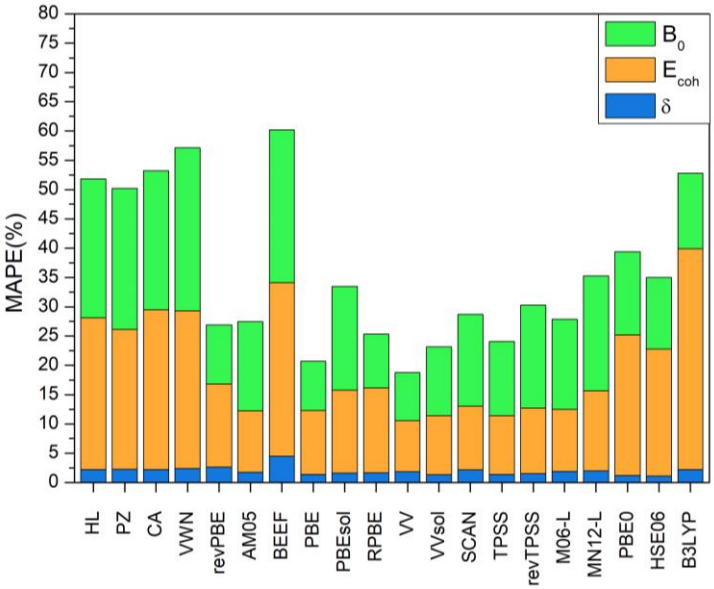

Figure 4. MAPE errors for the different *xc* functionals, here explored, or studied and available in the literature.[5-7,10]

Structure	Element	Surface	revPBE	Exp.
bcc	Fe	(001)	5.60	2.48
		(011)	6.86	
		(111)	3.03	
fcc	Cu	(001)	1.29	1.83
		(011)	1.33	
		(111)	0.97	
hcp	Ti	(0001)	1.87	2.10
		$(10\bar{1}0)$	1.90	
		$(11\bar{2}0)$	1.87	

Table 7. Surface energies, in $J \cdot m^{-2}$, obtained with the revPBE *xc* functional, as well as experimental values,[7] for the exemplary cases of Fe, Cu, and Ti.

The MAPE errors with respect the experimental values, collected from the literature,[7] are shown in Table 10, and visually, in Figure 5. Curiously, and opposite to bulk properties, it seems as LDA approaches provide better surface estimates, particularly for surface energies, see for

instance the values of VWN in Table 10. The GGA *xc* functionals provide a somewhat worse description; see PBE, PBEsol, RPBE, and revPBE, with the sole exception of VV and VVsol, which deliver better estimates, as a results of their adjustment to TM properties, fact that poses them as the best choices, being VV the best one concerning surface properties.

Structure	Element	Plane	revPBE	Exp.
bcc	Fe	(001)	3.82	3.82
		(011)	4.71	4.71
		(111)	3.88	3.88
fcc	Cu	(001)	4.46	4.46
		(011)	3.95	3.95
		(111)	4.21	4.21
hcp	Ti	(0001)	3.93	3.93
		$(10\bar{1}0)$	3.59	3.59
		$(11\bar{2}0)$	2.58	2.58

Table 8. Work functions, in eV, obtained with the revPBE *xc* functional, as well as experimental values,[7] for the exemplary cases of Fe, Cu, and Ti.

Finally, as far meta-GGA xc functionals are concerned, in this case TPSS, its added MAPEs are of the same height of the worst GGA case, in this case, the RPBE, thus, being its performance better for surface properties than for bulk properties. In any case, the revPBE functional performance is not considered in between the best. Indeed, when one joints bulk and surface MAPEs, as seen in Figure 6, the best overall functional is VVsol, closely followed by VV, in concordance with the literature.[10] Thus, revPBE xc functional is not a overall improvement, although, to be honest, one should carry out the surface analysis on other promising xc functionals, like AM05 or SCAN.

Structure	Element	Plane	δ_{ij}	revPBE	Exp.
bcc	Fe	(001)	12	-21.68	-1.4
			23	-7.57	
			34	-6.04	
		(011)	12	-5.04	1
			23	0.34	0.5
			34	0.34	
		(111)	12	-99.07	-16.9
			23	-99.28	-9.8
			34	14.19	-1.4
fcc	Cu	(001)	12	-2.40	-1.1
			23	0.55	1.7

			34	-0.17	
		(011)	12	-9.92	-10
			23	4.40	0
			34	-1.77	
		(111)	12	-0.87	-0.7
			23	0.03	
			34	-0.04	-1.1
hcp	Ti	(0001)	12	-7.69	-4.9
			23	2.97	-1.4
			34	-2.14	16
		$(10\bar{1}0)$	12	0.65	
			23	-8.65	
			34	12.80	
		$(11\bar{2}0)$	12	3.85	
			23	5.74	
			34	8.89	

Table 9. Interlayer distances, Δ_{ij}, in eV, obtained with the revPBE *xc* functional, as well as experimental values,[7] for the exemplary cases of Fe, Cu, and Ti.

xc	γ	ϕ	Δ_{ij}	**Sum**
VWN	13.48	22.85	11.51	47.84
PBEsol	16.58	21.42	10.87	48.87
PBE	27.11	20.77	10.11	57.99
RPBE	34.84	22.04	10.36	67.24
VV	22.01	6.57	20.66	49.24
VVsol	14.76	6.43	22.27	43.46
revPBE	31.86	16.72	7.32	55.90
TPSS	31.42	22.41	13.76	67.59

Table 10. MAPE errors from *xc* functionals for different steps in Jacob's Ladder for γ, in J·m^2, work functions, in eV, and δ_{ij} in Å.

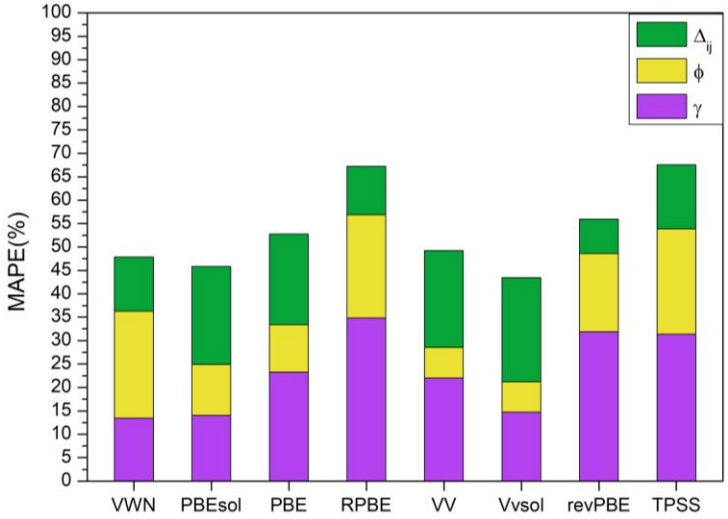

Figure 5. Added MAPEs for the δ_{ij}, ϕ, and γ, properties, for each of the different explored *xc*, as well as cases reported in the literature.[7,10]

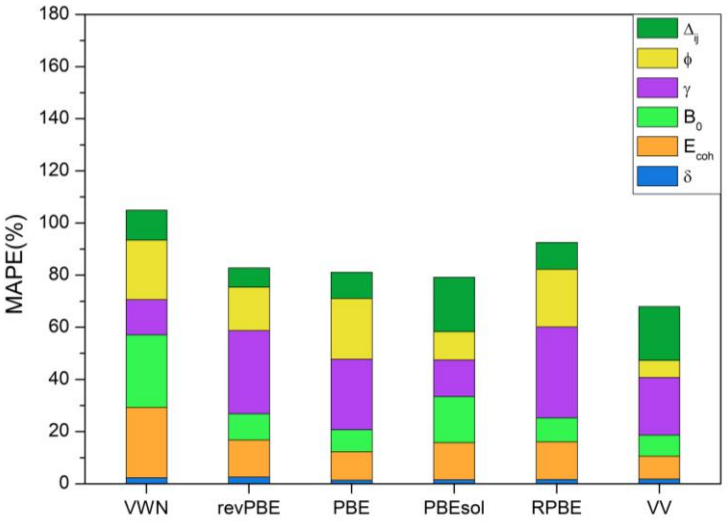

Figure 6. MAPE errors for the different *xc* functionals, either here explored, or studied and available in the literature for bulk and surfaces properties.[5-7,10]

7. CONCLUSIONS

In light of the presented and discussed results, as exposed in the previous section, one can extract the following clear conclusions.

- All the here studied functionals (HL, PZ, revPBE, AM05, SCAN, and BEEF) are suited in optimizing TM bulk structures, with no apparent artefact results.
- The revPBE functional is found to be the best in describing bulk, δ, E_{coh}, B_0 properties from the explored *xc*, closely followed by AM05 GGA, and as well as by SCAN meta-GGA. LDA functionals are not advised for such systems, because, even if excellent at determining bond lengths, they systematically overestimate bond strengths.
- Machine learned BEEF *xc* functional is found to be the worst explored case, with errors in the order of the LDA, a point which puts the question mark in whether such a functional was properly developed, or contains limitations in its definition.
- Present SCAN bulk estimates display a very god agreement with other previous calculations in the literature,[29] also showing that enlarging the basis set and the **k**-point sampling is beneficial for the accuracy.
- None of the newly functionals display better accuracy than VV functional,[10] specifically developed to describe bulk TMs.
- When accounting for surface properties, revPBE somewhat impoverishes its description, as is still far from best developed functional when according both bulk and surface properties, the VVsol.[10]

8. REFERENCES

1. Ceperley, D. M.; Alder, B. J. Ground State of the Electron Gas by a Stochastic Method. *Phys. Rev. Lett.* **1980,** *45,* 566–569.
2. Perdew, J. P.; Schmidt, K. Jacob's Ladder of Density Functional Approximations for the Exchange-Correlation Energy. *AIP Conf. Proc.* **2000**, *577*, 1.
3. Städele, M.; Moukara, M.; Majewski J. A.; Vogl, P.; Görling, A. Exact Exchange Kohn-Sham Formalism Applied to Semiconductors. *Phys. Rev. B* **1999,** *59*, 10031-10043.
4. Medvedev, M. G.; Bushmarinov, I. S.; Sun, J.; Perdew, J. P.; Lyssenko, K. A. Density Functional Theory is Straying from the Path toward the Exact Functional. *Science* **2017**, *355*, 49-52.
5. Janthon, P.; Luo, S.; Kozlov, S. M.; Viñes, F.; Limtrakul, J.; Truhlar, D. G.; Illas, F. Bulk Properties of Transition Metals: A Challenge for the Design of Universal Density Functionals. *J. Chem. Theory Comput*. **2014,** *10,* 3832-3839.
6. Janthon, P.; Luo, S.; Kozlov, S. M.; Viñes, F.; Limtrakul, J.; Illas, F. Establishing the Accuracy of Broadly Used Density Functionals in Describing Bulk Properties of Transition Metals. *J. Chem. Theory Comput.* **2013,** *9,* 1631-1640.
7. Vega, L.; Ruvireta, J.; Viñes, F.; Illas, F. Jacob's Ladder as Sketched by Escher: Assessing the Performance of Broadly Used Density Functionals on Transition Metal Surface Properties. *J. Chem. Theory Comput*. **2018**, *14*, 395-403.
8. Perdew, J. P.; Burke, K.; Ernzerhof, M. Generalized Gradient Approximation Made Simple. *Phys. Rev. Lett.* **1996**, *77*, 3865-3868.
9. Cramer, C. J.; Truhlar, D. G. Density Functional Theory for Transition Metals and Transition Metal Chemistry. *Phys. Chem. Chem. Phys.* **2009**, *11*, 10757-10816.
10. Vega, L.; Viñes, F. Generalized Gradient Approximation Adjusted to Transition Metals Properties: Key Roles of Exchange and Local Spin Density. *J. Comput. Chem.* **2020**, *41*, 2598–2603.
11. Sun, J.; Ruzinsky, A.; Perdew, J. P. Strongly Constrained and Appropriately Normed Semilocal Density Functional. *Phys. Rev. Lett.* **2015**, *115*, 036402.
12. Sun, J.; Marsman M.; Csonka, G. I.; Ruzsinsky. A.; Hao P.; Kim, Y.; Kresse, G.; Perdew, J. P.; Self-Consistent Meta-Generalized Gradient Approximation within the Projector-Augmented-Wave Method. *Phys. Rev. B* **2011**, *84,* 035117.
13. Hedin, L.; Lundqvist, B. I. Explicit Local Exchange-Correlation Potentials *J. Phys. C* **1971**, *4*, 2064.
14. Perdew, J. P.; Zunger, A. Self-Interaction Correction to Density-Functional Approximations for Many-Electron Systems. *Phys. Rev. B* **1981**, *23*, 5048.
15. Armiento, R.; Mattsson, A. E. Functional Designed to Include Surface Effects in Self-Consistent Density Functional Theory. *Phys. Rev. B* **2005**, *72*, 085108.
16. Zhang, Y.; Yang, W. Comment on "Generalized Gradient Approximation Made Simple". *Phys. Rev. Lett*. **1998**, *80*, 89017. Hohenberg, P.; Kohn, W. Inhomogeneous electron gas. *Phys. Rev.* **1964**, *136*, 864–871.
17. Hohenberg, P.; Kohn, W. Inhomogeneous Electron Gas. *Phys. Rev.* **1964**, *136*, B864.
18. Kohn, W.; Sham, L. Self-Consistent Equations Including Exchange and Correlation Effects. *Phys. Rev.* **1965**, 140, 1133–1138.
19. Kohn, W.; Sham, L. J. Self-Consistent Equations Including Exchange and Correlation Effects. *Physical Review* **1965**, *140*, A1133-A1138.

20. Wellendorf, J.; Lundgaard, K. T.; Mogelhoj, A.; Petzold, V.; Landis, D. D.; Nørskov, J. K.; Bligaard, T.; Jacobsen K. W. Density Functionals for Surface Science: Exchange-Correlation Model Development with Bayesian Error Estimation. *Phys. Rev. B* **2012**, *85*, 235149.
21. Adamo, C.; Barone, V. J. Toward reliable density functional methods without adjustable parameters: The PBE0 model. *Chem. Phys.* **1999**, *110*, 6158.
22. Krukau , A. V.; Vydrov, O. A.; Izmaylov, A. F.; Scuseria, G. E. Influence of Exchange Screening Parameter on the Performance of Screened Hybrid Functionals. *J. Chem. Phys.* **2006**, *125*, 224106.
23. Paier J.; Marsman M.; Kresse, G. Why Does the B3LYP Hybrid Functional Fail for Metals? *J. Chem. Phys.* **2007**, *127*, 024103.
24. Notario-Estévez, A.; Kozov, S. M.; Viñes, F.; Illas, F. Electronic-Structure-Based Material Descriptors: (In)dependence on Self-Interaction and Hartree-Fock Exchange. *Chem. Commun*. **2015**, *51*, 5602-5605.
25. Kresse, G.; Furthmüller, J. Efficient Iterative Schemes for *Ab Initio* Total-Energy Calculation Using Plane-Wave Basis Set. *Phys. Rev. B* **1996,** *54*, 11169-11186.
26. Blöchl, P. E. Projector augmented-wave method. *Phys. Rev. B* **1994**, *50*, 17953.
27. Blöchl, P. E.; Jepsen, O.; Andersen, O. K. Improved Tetrahedron Method for Brillouin-Zone Integrations. *Phys. Rev. B* **1994**, *49*, 16223-16233.
28. Lejaeghere, K.; Van Speybroeck, V.; Van Oost, G.; Cottenier, S. Error Estimates for Solid-State Density-Functional Theory Predictions: An Overview by Means of the Ground-State Elemental Crystals. *Crit. Rev. Solid State Mater. Sci.* **2014**, *39*, 1-24.
29. Jana, S.; Sharma, K.; Samal, P. Assessing the Performance of the Recent meta-GGA Density Functionals for Describing the Lattice Constants, Bulk Moduli, and Cohesive Energies of Alkali, Alkaline-Earth, and Transition Metals. *J. Chem. Phys*. **2018**, *149*, 164703.
30. Vosko, S. H.; Wilk, L.; Nusair, M. Accurate Spin-Dependent Electron Liquid Correlation Energies for Local Spin Density Calculations: A Critical Analysis. *Can. J. Phys.* **1980**, *58*, 1200-1211.
31. Perdew, J. P.; Ruzsinszky, A.; Csonka, G. I.; Vydrov, O. A.; Scuseria, G. E.; Constantin, L. A.; Zhou, X.; Burke, K. Restoring the Density-Gradient Expansion for Exchange in Solids and Surfaces. *Phys. Rev. Lett.* **2008**, *100*, 136406.
32. Hammer, B.; Hansen, L. B.; Nørskov, J. K. Improved Adsorption Energetics within Density-Functional Theory Using Revised Perdew-Burke-Ernzerhof Functionals. *Phys. Rev. B* **1999**, *59*, 7413-7421.
33. Zhao, Y.; Truhlar, D. G. A New Local Density Functional for Main-Group Thermochemistry, Transition Metal Bonding, Thermochemical Kinetics, and Noncovalent Interactions. *J. Chem. Phys.* **2006**, *125*, 194101.
34. Peverati, R.; Truhlar, D. G. An Improved and Broadly Accurate Local Approximation to Exchange-Correlation Density Functional: The MN12-L Functional for Electronic Structure Calculations in Chemistry and Physics. *Phys. Chem. Chem. Phys.* **2012**, *14*, 13171-13174.
35. Heyd, J.; Scuseria, G. E.; Ernzerhof, M. Hybrid Functionals Based on a Screened Coulomb Potential. *J. Chem. Phys.* **2003**, *118*, 8207.
36. Becke, A. D. Density-Functional Thermochemistry III. The Role of Exact Exchange. *J. Chem. Phys.* **1993**, *98*, 5648.